SPACE WEATHER, VOL. 4, S06007, doi:10.1029/2005SW000177, 2006

Click Here for Full Article

Specification of >2 MeV geosynchronous electrons based on solar wind measurements

E. Burin des Roziers[1] and X. Li[1]

Received 14 June 2005; revised 20 January 2006; accepted 6 March 2006; published 28 June 2006.

[1] Relativistic electron flux measurements from geosynchronous satellites show a local time dependence. This local time dependence is due to the radial profile of the electron fluxes and the dayside/nightside asymmetry of the Earth's magnetosphere and is also affected by geomagnetic activity, which is in turn affected by the solar wind. Statistical asynchronous regression (SAR), a statistical method recently adapted for magnetospheric studies, was used to determine the relationship between electron fluxes measured at different local times, as a function of the *Kp* index (O'Brien et al., 2001). In this study, we use measurements directly from the solar wind, instead of the *Kp* index, and the SAR method as the basis for determining the local time dependence of geosynchronous energetic electron fluxes. We use solar wind parameters as input in our model to map GOES 10 > 2 MeV electron measurements to other local times and compare them with electron measurements from five widely spaced LANL geosynchronous satellites when they pass through these local times. We cross calibrate the electron measurements from the five LANL satellites and find that the averaged electron flux from individual satellites can differ by up to 50% even though the particle detectors were identically designed. In this study, we normalize measurements from each LANL spacecraft to the average value of all five LANL spacecraft. We also cross calibrate the electron measurements from the LANL satellites and from GOES 10 and find that the energy spectrum is best described by a power law index which is a function of the current average LANL 1.1–1.5 MeV electron flux level. We explore the effects of solar wind velocity, dynamic pressure, and density on the local time dependence of geosynchronous electron fluxes. We find that for the given 4.3 year data set, using only solar wind velocity gives rise to the best results. We check the efficacy of the model by mapping GOES 10 > 2 MeV electron measurements at other local times to local noon and comparing with electron measurements from LANL satellites when they pass through local noon: We achieve an out-of-sample prediction efficiency (PE) of 0.83 and a linear correlation coefficient (LC) of 0.93 for January 2000, whereas we achieve a PE of 0.81 and LC of 0.92 for the year 2000. The PE and LC are different when mapping GOES 10 > 2 MeV electron measurements at one local time to other local times, with the highest PE around prenoon and afternoon and the lowest near midnight.

Citation: Burin des Roziers, E., and X. Li (2006), Specification of >2 MeV geosynchronous electrons based on solar wind measurements, *Space Weather*, *4*, S06007, doi:10.1029/2005SW000177.

1. Introduction

[2] As the number of satellites (scientific, military and commercial) increases, so does the importance of understanding the environment in which these satellites reside. Successfully predicting space weather becomes not only an important scientific goal, but also an essential tool to protect the spaceborne technology on which society now depends. Both sudden enhancements in and prolonged exposure to energetic particles in the Earth's radiation belts can cause satellite malfunctions and failures. Satellite operators need to know such particle fluxes to explain and prevent these malfunctions. This paper describes an empirical model of the local time dependence of energetic geosynchronous electrons based on solar wind measurements. With an electron flux measurement from a single geosynchronous satellite and the solar wind as input, this model provides the most likely electron flux at any local time around geosynchronous orbit.

[1]Department of Aerospace Engineering, University of Colorado, Boulder, Colorado, USA.

Copyright 2006 by the American Geophysical Union

[3] The radiation belts consist of protons and electrons, with energies from hundreds of keV to several MeV, trapped in the Earth's magnetic field. In general, the belts can be divided into the inner belt and the outer belt, separated by an area of low flux known as the slot region. The inner belt, consisting mainly of protons, is relatively stable and varies on solar cycle timescales. The outer belt consists primarily of electrons and is characterized by large flux variations on much shorter timescales [*Li and Temerin*, 2001]. The outer belt ranges from about 3 R_E to the last closed field line, and usually has a radial peak in electron flux around L = 4, where L would be equivalent to geocentric distance (R_E) near the equator for a dipole field.

[4] Particles trapped in the magnetosphere move on drift shells (or L shells) that correspond to contours of constant magnetic field at their mirror points, where the particle's pitch angle, the angle between the particle's velocity and the local magnetic field line, is 90°. In a compressed dipolar field, such as the magnetosphere, drift shells are asymmetric (particularly near the equatorial region), being farther from the Earth on the dayside and closer on the nightside. As a result, geocentric distance and the L shells of particles are not equivalent, as demonstrated in Figure 1.

[5] For example, a satellite in geosynchronous orbit (~6.6 R_E) at midnight may measure electrons on a drift shell that corresponds to L = 7, while a geosynchronous satellite at noon may measure electrons on a drift shell closer to L = 5. The radial flux profile of radiation belt electrons, whose maximum is usually around L = 4, has a peak closer to geosynchronous orbit on the dayside. As a result of this asymmetry, geosynchronous satellite measurements usually show higher electron flux on the dayside than on the nightside. This dayside-nightside asymmetry can be seen in Figures 2a and 2b, which show one year averaged GOES 10 measurements of >2 MeV geosynchronous electron flux and total magnetic field magnitude, respectively, versus local time.

[6] The extent of this asymmetry, and therefore of the noon/midnight electron flux ratio, depends on solar wind conditions. It was discovered early [*Williams*, 1966] that the solar wind velocity played an important role in the modulation of radiation belt electrons. Later, *Paulikas and Blake* [1979] found a quantitative correlation between geosynchronous electron fluxes and high-speed solar wind streams: they showed that the electron flux enhances 1 to 2 days after the passage of a high-speed solar wind stream. In addition, increasing the solar wind dynamic pressure usually increases the noon/midnight electron flux ratio. However, if the dynamic pressure is large enough to push the magnetopause inside geosynchronous orbit, a geosynchronous satellite near local noon will exit the magnetosphere and measure a significant decrease in electron flux. Therefore knowledge of the magnetospheric configuration, which largely depends on the solar wind, is vital to understanding geosynchronous energetic electrons.

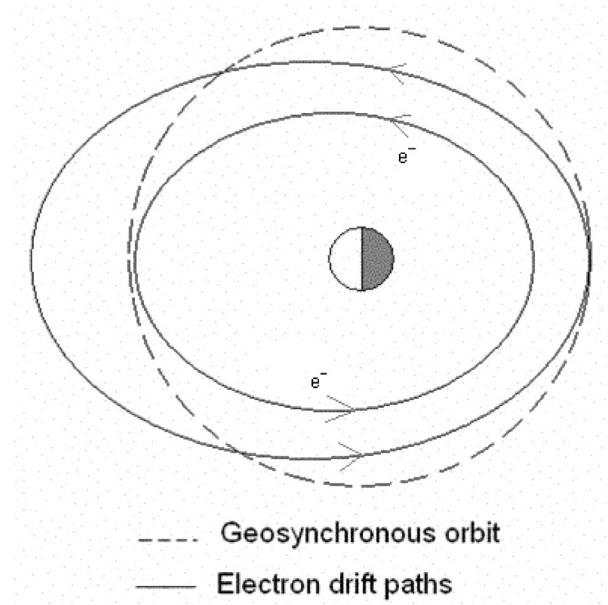

Figure 1. Cartoon comparing geosynchronous orbit (dashed curve) and equatorially mirroring electron drift paths (solid lines). Because of the asymmetry of the Earth's magnetosphere, electrons drift farther from the Earth on the dayside. As a result, a geostationary spacecraft measures electrons on different drift shells depending on the spacecraft's local time.

[7] Satellite designers rely on radiation belt models to design spacecraft capable of withstanding the near-Earth space environment. The most widely used empirical model is the AE 8 trapped electron radiation belt model developed by NASA [*Vette*, 1966, 1991]. The AE 8 model is a quasi-static model developed on the basis of observations, which provides electron flux estimates in the inner belt, slot region and outer belt separately. An energy and L shell–dependent sinusoidal local time dependence has been added to improve the estimates, but these are meant to represent long-time-averaged conditions, and do not capture the high local time variability of outer belt electrons [*Spjeldvik and Rothwell*, 1985; *Li*, 2002].

[8] Another empirical radiation belt model is the CRRESELE model [*Brautigam and Bell*, 1995]. This model was developed on the basis of observations from the CRRES spacecraft and provides a three-dimensional picture of the outer zone electrons. It has been shown [*Brautigam et al.*, 1992] to represent the outer zone electrons more accurately than the AE 8 model, but it assumes azimuthal symmetry. Neither of these models includes solar wind as inputs.

[9] *Li* [2004] and *Li et al.* [2001] developed a model that predicts daily averaged geosynchronous electron fluxes, based solely on solar wind inputs (a real-time forecast of electron fluxes based on this model can be found online at

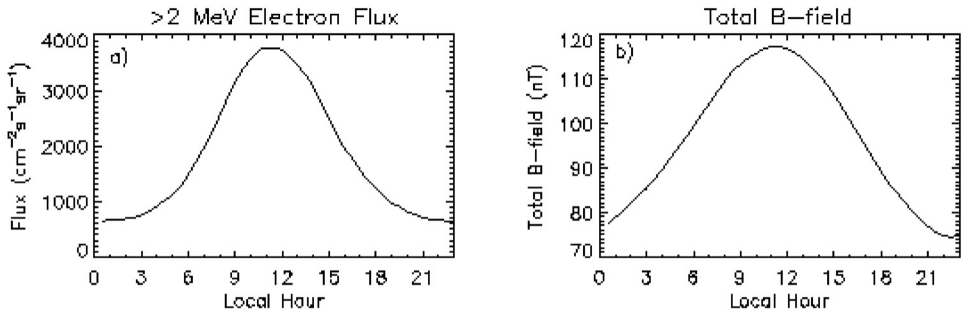

Figure 2. (a) GOES 10 > 2 MeV electron measurements averaged over 30 min for the year 2000 as a function of local time. (b) GOES 10 total magnetic field magnitude averaged over 30 min for the year 2000 as a function of local time.

http://lasp.colorado.edu/∼lix). However, because of the longitudinal asymmetry of the magnetosphere, the geosynchronous electron flux at local noon is, on average, more than five times greater than the electron flux at local midnight. During geomagnetically active times, this ratio can be much larger. It is therefore important to understand how the local time dependence of geosynchronous electron fluxes varies with the solar wind. In addition, it is also desirable for spacecraft engineers and operators to know the temporal variations of the average electron fluxes as well as the electron fluxes at any local time, for a given universal time.

[10] *O'Brien et al.* [2001] used a statistical data analysis method called statistical asynchronous regression (SAR) to determine the local time dependence of geosynchronous energetic electrons, based on the *Kp* index, a measure of geomagnetic activity. Using archived data from several LANL and GOES spacecraft, they were able to model the flux that a stationary satellite would measure at local noon and compared the result with actual measurements from GOES 8, when it was at local noon.

[11] Since geomagnetic activity depends on the solar wind, an analysis similar to that of *O'Brien et al.* [2001] can determine the local time dependence of geosynchronous energetic electron fluxes based directly on the solar wind. Such a model would allow us to determine the local time dependence in real time and also determine which parameters in the solar wind have the greatest effect on the flux local time dependence.

[12] Before showing our specification results of >2 MeV electron fluxes at different local times, we will first describe in detail the cross calibration and normalization of the electron data from a suite of spacecraft at geosynchronous orbit. Then, we will describe the development of our specification model on the basis of the SAR method. Finally, we discuss the results.

2. Data and Data Handling

[13] In this study, we use >2 MeV electron flux measurements from the Energetic Particle Sensor (EPS) on the geosynchronous spacecraft GOES 10 [*Onsager et al.*, 1996] as input to the model, as well as electron flux measurements from the SOPA instruments on five LANL geosynchronous spacecraft [*Belian et al.*, 1992] for comparison of the model results. Solar wind measurements were taken from the ACE spacecraft, orbiting around the L1 point in the solar wind about 235 R_E upstream from the Earth [*Stone et al.*, 1998]. Our model requires GOES 10 and solar wind measurements for the same time period. The overlap period of our data starts on 21 March 1999 and ends on 8 September 2003. We omit GOES 10 and solar wind data gaps from our study. In order to validate our results, we compare our model output with LANL measurements, which are available from 2 January 2000 to 20 September 2002.

[14] This study requires simultaneous measurements from several spacecraft. A meaningful comparison among measurements from different spacecraft requires measurements from these spacecraft to be cross calibrated and converted into a uniform format. This is a challenge since the averaged electron fluxes from identically designed instruments can be quite different.

2.1. Calibration of LANL Measurements

[15] The first step of converting all data to a uniform format involves the LANL instruments alone. Although the LANL instruments were identically designed, long-term-averaged measurements from different instruments can still differ by up to 50%, as shown in Figure 3a. The LANL spacecraft were also designed to have identical orbits, so we assume that this difference is due to instrumental effects (G. Reeves, private communication, 2004). As a result, we normalize LANL electron flux measurements from the 1.1 to 1.5 MeV energy channel by the following method: first we average the measurements from each spacecraft over the entire time period (approximately 2 years), and then normalizing each to the average of all five LANL spacecraft. The resulting normalization factors for each spacecraft were kept constant throughout the study and are provided in Table 1. Including these normalization factors improved the correlation between measurements from different LANL spacecraft, as shown

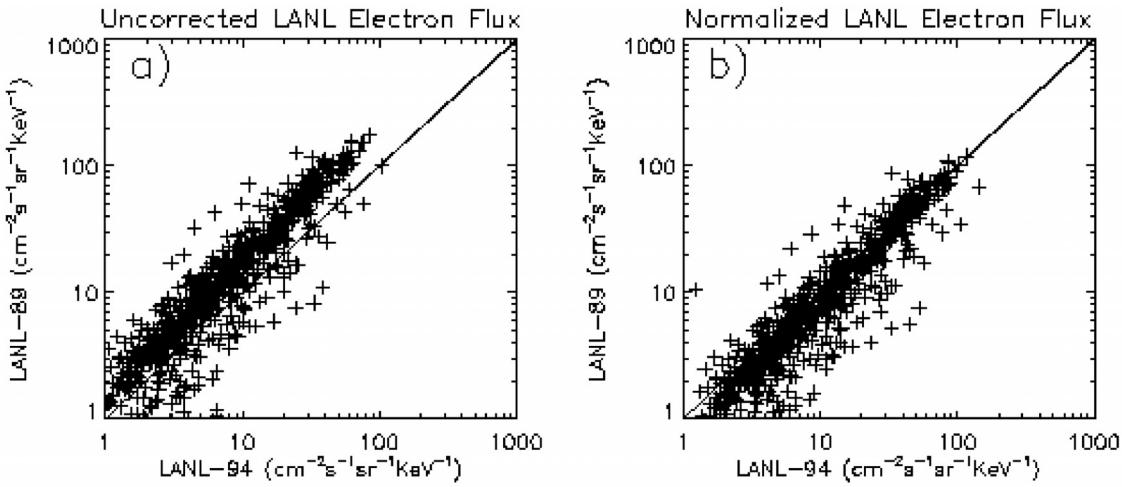

Figure 3. Scatterplots of daily averaged LANL 89 versus daily averaged LANL 94 1.1−1.5 MeV electrons (left) before normalization and (right) after normalization. Normalization factors were found by taking measurements averaged over the entire time period (~2 years) from each spacecraft and normalizing each to the average of all five LANL spacecraft. The right plot shows that this correction improved the correlation from one LANL spacecraft to another.

in Figure 3b. These normalization factors were calculated without considering the different magnetic latitudes of the LANL spacecraft. As discussed in the following section, the various magnetic latitudes of the LANL spacecraft have little effect on the LANL flux measurements and on the normalization factors.

2.2. Cross Calibration of LANL and GOES Measurements

[16] Even though the LANL and GOES spacecraft are in geosynchronous orbits, each spacecraft is located at a slightly different magnetic latitude. If a satellite is not on the geomagnetic equator, the instrument will not detect a particle mirroring at or near the equator. This effect is accounted for by assuming a pitch angle distribution of the form

$$j \propto \sin^n \alpha, \tag{1}$$

where j is the flux, α is the pitch angle, and n is a fitting parameter. *Vampola* [1998] found that, on average, the pitch angle distribution near geosynchronous orbit can be well approximated by letting $n = 1$. Using this assumption and a dipole field model, we map flux measurements from all instruments to the geomagnetic equator. Since all LANL and GOES spacecraft are within 11.6° of the magnetic equator, this correction factor is <1%.

2.3. Energy Spectrum

[17] Although our model uses GOES 10 integral electron fluxes ($E > 2$ MeV) as input, we validate our results with LANL differential electron flux measurements (1.1 MeV < E < 1.5 MeV). As a result, an appropriate energy spectrum needs to be used to convert the LANL differential flux channel to the GOES 10 integral flux channel. The energy spectrum is assumed to be of the form

$$j = AE^{-\gamma}, \tag{2}$$

where j is the differential flux measured at some energy, E, γ is the power law index (always positive) that determines the hardness of the spectrum, and A is a scaling constant. We found that γ is a function of the LANL 1.1−1.5 MeV electron flux level. During times of low electron fluxes, there are relatively few high-energy electrons, so the energy spectrum during these times will have a larger γ. Alternatively, during times of high electron fluxes, the presence of more high-energy electrons may raise the tail of the energy spectrum and decrease the power law index, γ. To determine an appropriate form of γ as a function of the LANL electron flux level, LANL SOPA fluxes from the three highest differential energy channels were first sorted by five different LANL flux levels, averaged over the five spacecraft. A different power law index, γ, was fitted to each resulting energy spectrum, thus providing a tabular form of γ as a function of LANL flux levels. Next, an

Table 1. Normalization Factors for LANL Spacecraft

Spacecraft	Normalization Factor
LANL 89	0.6846
LANL 90	1.1395
LANL 91	0.8823
LANL 94	1.2561
LANL 97	1.3660

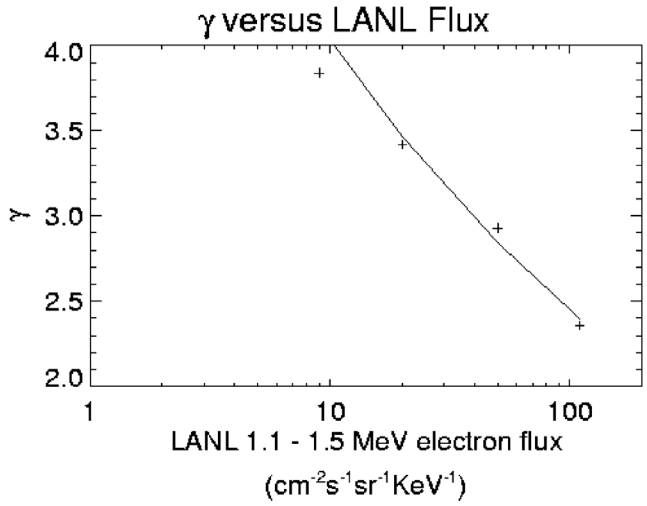

Figure 4. Plot of the empirically determined varying power law index as a function of LANL 1.1–1.5 MeV electron flux, averaged over five LANL spacecraft. This function was determined by sorting LANL fluxes from three different energy channels by five different LANL flux levels. A different power law index was fitted to each resulting energy spectrum, thus providing a tabular form of the power law index as a function of LANL flux, averaged over the five LANL spacecraft. An analytical function (solid curve) was fitted to this tabular form.

exponential function was fitted to this tabular form to provide an analytical function for γ as a function of LANL electron flux, as follows:

$$\gamma = aj^{-b}, \tag{3}$$

where j is the average of the five LANL spacecraft measurements of 1.1–1.5 MeV electron flux, and a and b are the fitting parameters, empirically determined to be 6.51 and 0.208, respectively. Figure 4 shows the resulting power law index, γ, versus average LANL electron flux of energy 1.1–1.5 MeV. This varying γ was used throughout the study to convert LANL differential flux to >2 MeV integral flux. Using this empirically determined, varying power law index, γ, led to immediate improvements in the comparison of daily averaged corrected LANL flux with GOES 10 flux, as shown in Figure 5. The outlying point above the $x = y$ line, near (20, 10000) in Figure 5b, corresponds to a measurement during the Bastille Day event, on 14 July 2000. There was a major solar proton event (SPE) on that day that contaminated the electron flux measurements with protons. A correction algorithm is applied to GOES 10 data in an attempt to correct for SPEs, while no such attempt is made for the LANL data. The LANL instrument is generally less sensitive to proton contamination. For low proton flux levels, there is no correlation between the LANL 1.1–1.5 MeV electrons and the 80–165 MeV protons measured by GOES 8. However, if the 80–165 MeV proton flux reaches a threshold of about 0.2 cm^{-2} s^{-1} sr^{-1} MeV^{-1}, there is a positive correlation between the LANL electron flux and the GOES 8 proton flux (S. Bourdarie, private communication, 2005). Of the 13 solar proton events that occurred in 2000, only 2 events (14 July 2000 and 8 November 2000) produced proton fluxes that exceed the threshold given above. In each case, there is a data gap in the GOES 10 electron flux measurements, and thus these time periods were not included in our prediction efficiency calculations.

2.4. Solar Wind Propagation

[18] This study requires solar wind parameters at the magnetopause location. A simple ballistic propagation scheme provides an approximation for the solar wind parameters at the magnetopause location based on measurements at the L1 point. We used 10-min resolution solar wind measurements for the calculation and a travel distance from the L1 point to a subsolar point 10 R_E from the Earth. In the case when a high-speed solar wind stream overtakes a slower moving solar wind, the parameters of the slower wind were replaced by the parameters of the fast moving stream. From 21 March 1999 to 8 September 2003, this happened less than 0.02% of the time.

2.5. Data Bins and Averaging

[19] For the final step in the data preparation process, we average the GOES 10 flux in bins of 30 min in local time, centered on each hour and half hour. The LANL and solar wind data are also averaged over the same 30-min bins as the GOES 10 data.

3. Specification Method: Statistical Asynchronous Regression (SAR)

[20] SAR is a statistical tool that allows one to determine the relationship between two time varying quantities that are not measured simultaneously, such as electron fluxes at different local times. SAR makes use of the fundamental principle that probability is conserved under a change of variables. With a knowledge of the distribution function of each variable and the statistical relationship between these two variables, given the value of one variable, we can determine the probability that the other variable is measured within a certain range. As a result, SAR provides a means of determining the necessary mapping function to map one variable to the other. In other words, determining an empirical relationship between the distribution functions of the fluxes at different local times allows us, given a flux measurement at one local time, to determine the most probable flux at a different local time.

[21] It is convenient to provide a graphical description of this method. Suppose we have nonsimultaneous measurements of two time varying quantities, $X(t)$ and $Y(t)$. Let $X(t)$ represent the flux versus time measured at one local time and $Y(t)$ be the flux versus time measured at a different

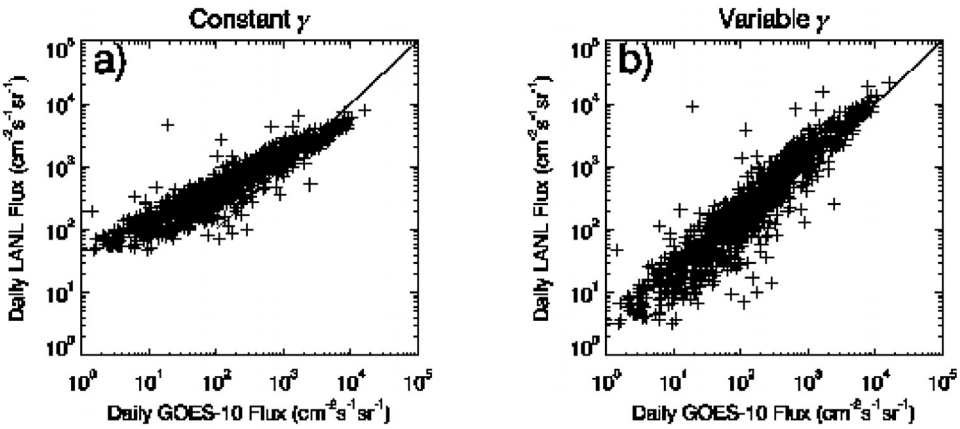

Figure 5. Scatterplots of daily GOES 10 flux versus daily LANL differential flux converted to >2 MeV electron flux: (a) result when using a constant power law index of 3.2 and (b) improved result when using the empirically determined varying power law index as a function of LANL flux.

local time, with x and y representing single measurements of $X(t)$ and $Y(t)$, respectively. We can construct the so-called complementary cumulative distribution function (CDF), $F(x)$, which represents the probability that a measurement of X will be greater than a given value, x. Similarly, we construct the complementary CDF, $G(y)$, which represents the probability that a measurement of Y will be greater than a given value, y. The objective is to find a mapping function, $y = u(x)$, with which we will be able to determine Y, the flux versus time at one local time, from X, the flux versus time at another local time. As an example, Figure 6 (inspired by Figure 9 from *O'Brien et al.* [2001]) shows actual complementary CDFs, $F(x)$ and $G(y)$, where $F(x)$ is the complementary CDF of the flux at local dawn (bottom solid curve) and $G(y)$ is the complementary CDF of the flux at local noon (top solid curve). As expected, there is a greater probability to measure a higher flux at noon than at dawn. This plot can be used to show how we retrieve the flux at local noon, given a measurement at local dawn. If we observe the flux at dawn to a certain value, x, we can move up from that value on the abscissa to $F(x)$, to read a probability. We then move horizontally, along that same probability, to $G(y)$, and down to the abscissa to read the value of the flux at noon corresponding to that probability, and therefore corresponding to the flux observed at noon. Mathematically, this process corresponds to

$$u(x) = G^{-1}[F(x)], \tag{4}$$

where $G^{-1}(y)$ is the inverse function of $G(y)$. This provides a method for determining the mapping function $u(x)$. As a result, SAR provides a means of determining the quantitative relationship between fluxes measured at different local times.

[22] In this study, we have determined such a relationship between the flux at local noon and the flux at other local times for a given solar wind condition. As a result, we have made this mapping function a function of solar wind parameters. Initially, we choose our two measured quantities to be the electron flux at local noon and the flux at dawn, for a specific solar wind condition. We estimate the complementary CDFs of the flux at each of these local times on the basis of historical observations by using the equations

$$\begin{aligned} F(x_i) &= \frac{i}{N_x} \\ G(y_j) &= \frac{j}{N_y}, \end{aligned} \tag{5}$$

where x_i is the ith smallest value in our data set of dawn fluxes and N_x is the total number of points in the set, and similarly, y_j is the jth smallest value in our data set of noon fluxes. Linear interpolation was used to determine the values of the CDF for the given flux level. The mapping function that relates the noon flux to the dawn flux can be recovered using the CDFs $F(x)$, $G(y)$, and equation (4). This method is repeated for other local times such that a set of mapping functions is accumulated, each relating the noon flux to the flux at a different local time, for a specified solar wind condition.

[23] As mentioned above, the relationship between the fluxes at different local times depends on the solar wind conditions, so this process must be repeated to determine a different set of mapping functions for every set of solar wind conditions. We now choose our measured quantities to be the fluxes measured during a second specified solar wind condition. We estimate the complementary CDFs of the flux at each local time and we use SAR to recover the mapping functions that relate the noon flux to the fluxes at other local times, for the new solar wind condition. In this manner, we develop a library of such mapping functions, which will allow us to determine the flux around geosynchronous orbit for a given universal time, given the flux at a single local time and the solar wind conditions at the same universal time.

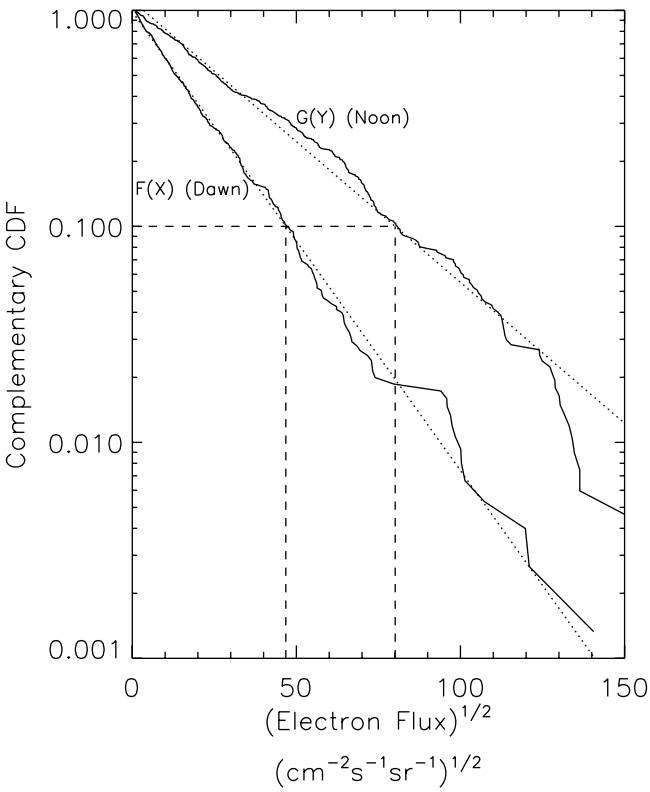

Figure 6. Graphical explanation of statistical asynchronous regression (SAR). The empirically determined complementary cumulative distribution functions (CDF) for the electron flux at local noon (top solid curve) and the flux at local dawn (bottom solid curve) are plotted along with their respective fits (dotted curves). The complementary CDF gives the probability (y axis) of measuring the flux higher than a given value (x axis). SAR provides a systematic way of retrieving the flux at noon, given a measurement of the flux at dawn.

[24] In the current study, we determine a mapping function for every solar wind velocity bin of width 25 km s^{-1}. The SAR model depends on a statistically significant number of GOES 10 measurements in a particular solar wind velocity bin for the mapping function to be valid. For the set of data used in this study, the statistics of the CDFs become low for solar wind velocities below 250 km s^{-1} and above 850 km s^{-1}. In this solar wind velocity range (250–850 km s^{-1}), we have accumulated 23 mapping functions, which allow us to map GOES 10 flux from one local time to any other local time.

4. Results and Discussion

[25] The objective of this work is to determine the local time dependence of geosynchronous energetic electron fluxes solely on the basis of solar wind parameters. *O'Brien et al.* [2001] applied the SAR method to geosynchronous electron fluxes using the *Kp* index as input. They were able to map GOES 8 flux to local noon with a prediction efficiency (PE) of 0.89 for the available data in the period from 7 March 1995 to 31 December 2000. We use the same method but using the solar wind as input. Using the solar wind as input allows us to understand which solar wind parameter is the most significant for the local time dependence of the MeV electrons and also allows us to make real-time specification of geosynchronous electrons, because of the readily available real-time solar wind measurements and GOES 10 data.

[26] The mapping functions described above were used to specify the >2 MeV geosynchronous electron fluxes that a stationary satellite at local noon would measure for the year 2000, given GOES 10 measurements around geosynchronous orbit and the solar wind conditions for the same year. We train our model with all available data in the intervals 21 March 1999 to 31 December 1999 and 1 January 2001 to 9 August 2003 and apply the model to the year 2000. The model needs to be trained with sufficient examples of different solar wind conditions. The year 1999 is in the ascending phase of the solar cycle. The year 2001, near the solar maximum, was a very active year and provides several examples of very high solar wind velocity. The years 2002 and 2003, during the descending phase, show recurring high-speed solar wind streams. Training the model using these time periods ensures that the model has multiple examples of various solar wind conditions. Figure 7 demonstrates the results, using a mapping function based only on solar wind velocity, for 10 days in January 2000. The resulting local noon electron flux was compared with LANL measurements, when the spacecraft was located at local noon. We calculate the prediction efficiency (PE) by using the equation

$$PE = 1 - \frac{\sum_{i=1}^{N} \left(\log(x_i) - \log(x_{pi})\right)^2}{\sum_{i=1}^{N} \left(\log(x_i) - \log(\bar{x})\right)^2}, \qquad (6)$$

where x_i is the flux observed by LANL at local noon, x_{pi} is the predicted flux at local noon, and $\bar{x}$ is the mean of the observed flux. The numerator of the above expression is commonly referred to as the mean square of the residual, and the denominator, as the variance. A PE of zero means that our prediction is as good as the average value of the flux at local noon, and a PE of 1 would result from a perfect prediction. The resulting out-of-sample prediction efficiency of 0.83 and a linear correlation of 0.93 for the month of January 2000 suggest that the solar wind velocity alone can specify most of the flux local time dependence. We see that, when GOES 10 is at local noon, the GOES 10 measurement exactly matches the flux predicted by the model. In addition, we observe that the model

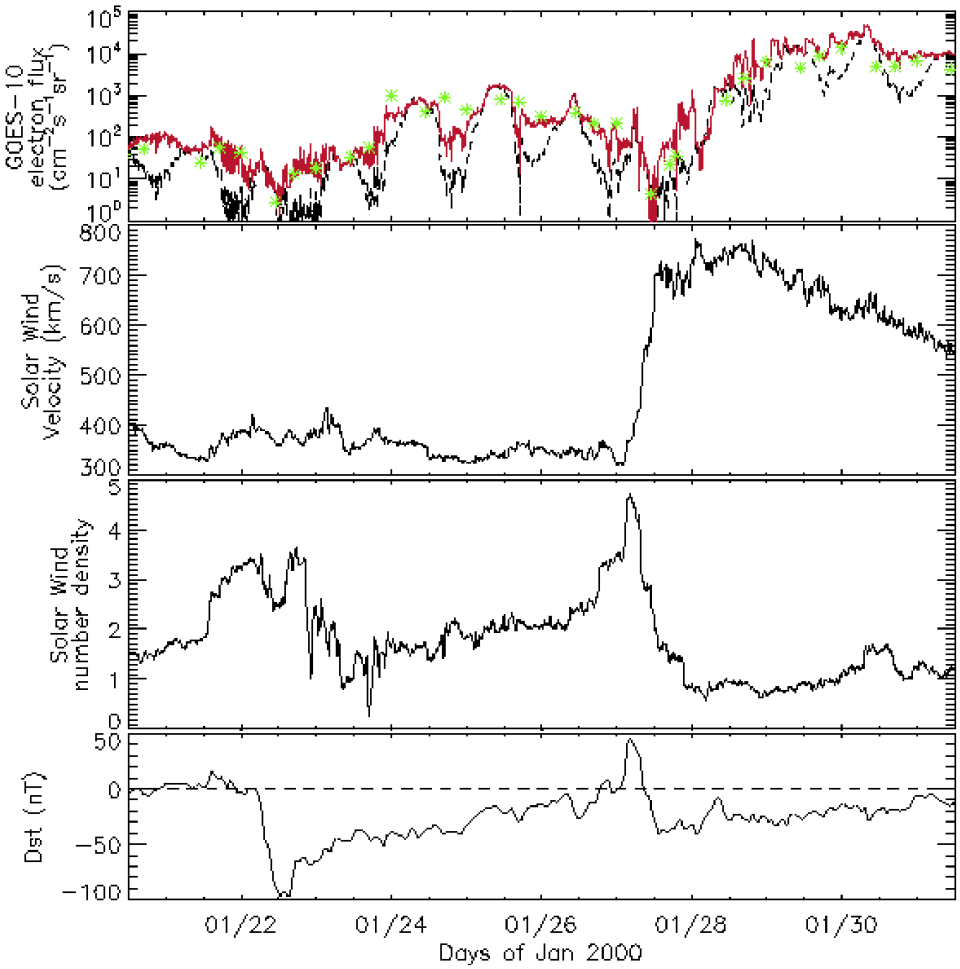

Figure 7. Example of 30-min averaged GOES 10 > 2 MeV electron flux (dashed curve) mapped to local noon (solid red curve) using the current solar wind velocity at the magnetopause. The model was trained with out-of-sample GOES 10 > 2 MeV electron flux measurements and applied to the year 2000. The local noon flux was compared to measurements from five LANL spacecraft as they passed through local noon (green asterisks). The PE is 0.81 for the year 2000 and 0.83 for the month of January 2000. Solar wind velocity, density, interplanetary magnetic field B_z (GSM), and the *Dst* index are provided for reference.

greatly reduces the diurnal variations due to the satellite orbit.

[27] Using the same method and a mapping function based only on solar wind velocity, we ran our model for the year 2000, and calculated a PE of 0.81 and a linear correlation coefficient (LC) of 0.92. The results of the model, plotted in Figure 8, show a clear correlation between the predicted and observed flux at local noon. The solid curve is the regression of the log of the predicted flux on the log of the observed flux and is given by the equation

$$\log(obs) = 0.933 \times \log(pred) + 0.028. \quad (7)$$

The dotted lines are the 3σ error bars, where σ^2 is defined as

$$\sigma^2 = \frac{1}{N}\sum_{i=1}^{N}(x_i - \bar{x})^2 \quad (8)$$

and represents the extent of the scatter of the data around the regression line. The correlation between the predictions and observations is demonstrated by predictions and observations, which are scattered in a narrow band around the regression line, over a broad range of flux (~5 orders of magnitude).

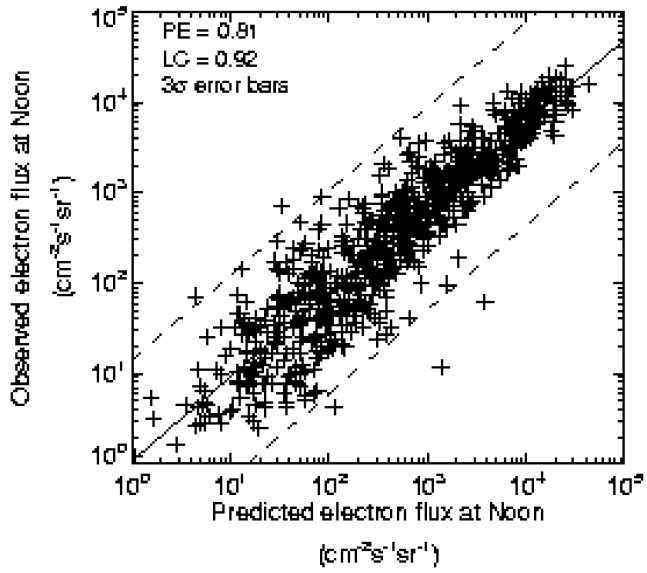

Figure 8. Results of the model applied to the year 2000: scatterplot of >2 MeV electron flux, averaged over 30 min, predicted at local noon versus that observed by five LANL spacecraft while they passed through local noon. The solid curve is the regression of the log of the prediction on the log of the observed flux. The dotted curves are the 3σ error bars. The PE is 0.81, and the LC is 0.92 for the year 2000.

4.1. Magnetopause Crossings

[28] The three outlying points, lying outside the 3σ error bars in Figure 8, are most likely due to the magnetopause moving inside geosynchronous orbit. If this occurs, the observed electron flux at noon will be much lower than the predicted flux at noon since our model does not take magnetopause crossings into account. If the magnetopause moves close to geosynchronous orbit, a study of Figure 1 shows that geosynchronous electrons on the nightside will encounter the magnetopause, while dayside geosynchronous electrons will not encounter the magnetopause unless it crosses geosynchronous orbit. Because of the statistical nature of our model, the model gives results that reflect the times when the magnetopause is close to, but still outside, geosynchronous orbit. For times when the magnetopause crosses geosynchronous orbit, the spacecraft near noon will be outside the magnetosphere and measure electron fluxes that are drastically reduced from magnetospheric measurements and our model will give poor results. For the point lying farthest away from the regression line, the LANL 94 spacecraft measured the observed flux as it passed through noon, on 27 November 2000, near 0500 UT. At that time, LANL 94 was at local noon and GOES 10 was near 0200 LT. The solar wind was very active prior to the LANL 94 reading at noon. The GOES 10 magnetometer shows clear evidence of a magnetopause crossing about 10 hours before the LANL 94 spacecraft was at local noon, about the time GOES 10 was on the dayside. There is a data gap in the LANL 94 measurement prior to this particular measurement and the LANL 94 data shows sharp and rapid (~1 hour, the time resolution of the data used in this study) fluctuations, which is not normally seen. In addition, during this measurement, the observed solar wind parameters (V_x = 575.2 km s^{-1}, IMF B_z = −0.39 nT, and P_{dyn} = 4.06 Pa) were used to calculate the magnetopause standoff distance, using the Petrinec and Russell magnetopause model [*Petrinec and Russell*, 1993, 1996], available on the Web (http://pixie.spasci.com/DynMod/). The magnetopause standoff distance was near 7.2 R_E, which supports the possibility of a magnetopause crossing near the time of the measurement.

[29] Similar arguments were used to identify the other two outlying points as possible magnetopause crossing events. It is likely that during other magnetopause crossings, our model predicts much higher flux than the observed flux at noon. From 21 March 1999 to 8 September 2003, using the Petrinec and Russell model with 30-min resolution solar wind inputs, we found the magnetopause passed within 6.6 R_E about 53 times, or approximately once per month. Implementing the magnetopause standoff distance in our model should further improve predictions during times of high solar wind dynamic pressure.

4.2. Other Solar Wind Parameters

[30] We have tried to use other solar wind parameters, such as solar wind dynamic pressure, as input to specify the electron fluxes at different local times. The solar wind velocity is the parameter that gives rise to the best results. Our model is statistical and empirical in nature. It requires a sufficient number of prior examples of certain solar wind conditions. GOES 10 may not have taken any measurements at a particular local time for a given extreme solar wind condition. In this case, we would not be able to train our model to handle such a solar wind condition, at this local time. As a result, the addition of other solar wind parameters (such as density, dynamic pressure, and B_z) did not increase the PE of the results most likely because they put more constraints on the solar wind inputs. Thus increasing the restrictions on the solar wind input by including other solar wind input parameters decreases the data samples used to train the model. We expect that, with more training data, adding solar wind input parameters may improve the overall prediction efficiency of the results.

4.3. Mapping to Other Local Times

[31] Because we can map the flux from any local time to local noon, it is also possible to map noon flux to any other local time. In this manner, given a measurement at one local time, we can now specify the flux at any other local time. Figure 9 shows the resulting prediction efficiencies (asterisks) and linear correlation coefficients (triangles) of mapping GOES 10 measurements to other local times.

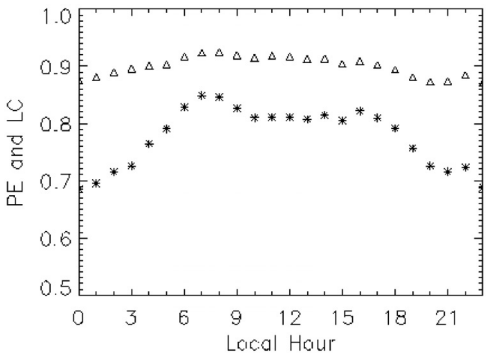

Figure 9. Results of the model applied to the year 2000 and mapped to all local hours. The prediction efficiency (asterisks) and linear correlation coefficient (triangles) are shown versus local hour.

[32] The prediction efficiencies on the nightside are consistently smaller than the prediction efficiencies on the dayside. The lowest prediction efficiency is found at midnight. This may be attributed to the fact that the variance of the flux at local midnight is consistently smaller than the variance at local noon, see Figure 10a (recall: $PE = 1 -$ mean squared residual/variance). Because the magnitude of the flux at local noon is generally larger than the fluxes at midnight, the deviations from the mean flux will also tend to be larger at noon than midnight. One might expect the same trend in the variance of the magnetic field around geosynchronous orbit. However, because of the highly variable magnetic conditions on the nightside, although the magnitude of the total magnetic field is small, its variance is rather significant on the nightside, as shown in Figure 10b. The nightside magnetic field near geosynchronous orbit is constantly stretched and then dipolarized, associated with enhanced magnetic activity. During the further stretching periods, a geosynchronous satellite might be significantly far away from the geomagnetic equator on the night side, and observe electrons populating significantly different L shells on successive orbits. As a result, it is much harder to predict the fluxes on the night side of geosynchronous orbit, and the residuals at midnight will be larger than at noon. All of these contribute to the lower PE at midnight than at other local times, though the LC is consistently high at all local times.

[33] The prediction efficiency at local noon is also lower than the prediction efficiencies at 0900 and 1600 LT. This may be due to magnetopause crossing events as described earlier. Magnetopause crossings would most affect electron flux observations near noon. We hope that including the *Petrinec and Russell*, 1993 magnetopause model in our model will increase the prediction efficiency near noon.

4.4. Comparison With the *O'Brien et al.* [2001] Model

[34] Although this work was inspired by the work done by *O'Brien et al.* [2001], there are four important differences between the two models that should be noted. First, O'Brien et al. used the *Kp* index as an input to the model. We use solar wind parameters as inputs, arguing that the *Kp* index is ultimately a function of the solar wind. Secondly, O'Brien et al. mapped GOES flux to noon and compared it to GOES 8 flux when the spacecraft was near noon. They similarly mapped LANL flux to noon and compared it to LANL 1994 flux when the spacecraft was near noon [*O'Brien*, 2001]. Because we compared GOES 10 flux with LANL flux, an accurate energy spectrum was needed to convert LANL differential flux to >2 MeV integral flux. Thirdly, in using the complementary cumu-

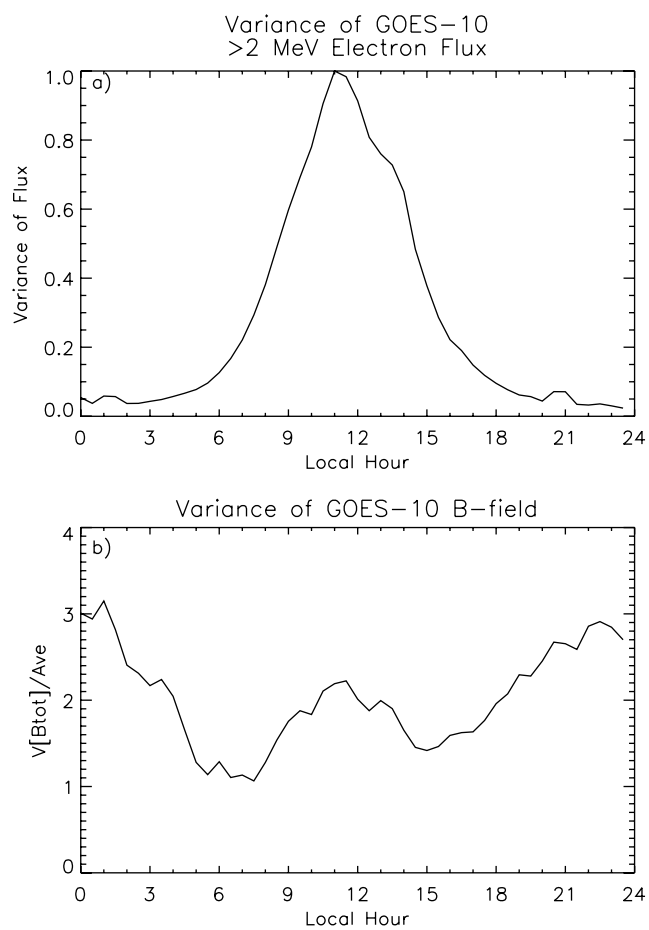

Figure 10. (a) Variance of GOES 10 > 2 MeV electron flux plotted versus local time. Since, in general, the electron flux has a larger magnitude at local noon, the variance is also larger at local noon. (b) Ratio of the variance to the average value of GOES 10 total magnetic field plotted versus local time. Since, in general, the magnitude of the magnetic field is larger at local noon, there is a peak in the variance around noon. However, because of the variable nature of the nightside magnetic field, as discussed in the text, the ratio is also significant on the nightside.

lative distribution functions (CDFs) estimated from the data, we linearly interpolated between points. O'Brien et al. fit a function to the CDFs of the form

$$P = Ae^{B\sqrt{j}}$$

where P is the probability of measuring the flux higher than a given flux value, j, and A and B are fit parameters. Although this form fits the CDFs well, there may be cases where the CDF is not well described by a particular analytical fit. Finally, O'Brien et al. used longer data sets (ranging from 1989 to 2000) from more spacecraft (4 GOES and five LANL spacecraft). A longer data set improves the statistics of the model.

5. Summary and Conclusions

[35] Our model uses the statistical asynchronous regression method to specify >2 MeV geosynchronous electron fluxes at different local times, given the solar wind condition at the magnetopause and an electron flux measurement at any other local time. In preparing the data sets for this study, we have cross calibrated the LANL satellites and determined that the energy spectrum is better defined by an empirically determined power law index which is a function of the current LANL 1.1–1.5 MeV electron flux, averaged over the five spacecraft. Using solar wind velocity as the only input and training the model with all available data in the periods from 21 March 1999 to 31 December 1999 and 1 January 2001 to 4 August 2003, we have been able to specify the local noon flux with a good out-of-sample PE of 0.83 and a LC of 0.93 for the month of January 2000 and an out-of-sample PE of 0.81 and LC of 0.92 for the year 2000. Adding other solar wind parameters as input produces results that are not as good as using only solar wind velocity, for the given data set. We also applied the same technique to specify the electron fluxes at other local times, resulting in different PEs, though the LC is consistently high at all local times. The prediction efficiencies are highest when specifying fluxes near prenoon and afternoon, and progressively decrease as the target local time approaches midnight. This is perhaps because it is harder to predict geosynchronous electron fluxes on the nightside because of the high variability of the magnetic field there.

[36] In the future, we would like to implement magnetopause crossings into our model and combine this model with the *Li* [2004] and *Li et al.* [2001] model, which predicts daily averaged geosynchronous electron fluxes on the basis of solar wind. Thus we would be able to predict electron fluxes everywhere around geosynchronous orbit on the basis of solar wind measurements and one current measurement of the electron flux.

[37] **Acknowledgments.** We thank T. P. O'Brien, S. Petrinec, G. Reeves, and T. Onsager and colleagues A. Barker and J. Gannon for helpful discussions. We thank the science teams (ACE/SWEPAM, ACE/Mag, GOES, and LANL) for making the data available. This work was supported in part by NASA grants (NAG5-10474 and -13518) and NSF grants (CISM and ATM-0233302).

References

Belian, R. D., G. R. Gisler, T. Cayton, and R. Christensen (1992), High Z energetic particles at geosynchronous orbit during the great solar proton event of October 1989, *J. Geophys. Res.*, *97*, 16,897.

Brautigam, D. H., and J. T. Bell (1995), CRRESELE documentation, *Tech. Rep. PL-TR-95-2128*, Phillips Lab., U.S. Air Force Materiel Command, Hanscom AFB, Mass.

Brautigam, D. H., M. S. Gussenhoven, and E. G. Mullen (1992), Quasi-static model of outer zone electrons, *IEEE Trans. Nucl. Sci.*, *39*, 1797.

Li, X. (2002), Radiation belt electrons and substorm injections, in *International Conference on Substorms-6 Proceedings*, edited by R. M. Winglee, p. 305, Univ. of Wash., Seattle.

Li, X. (2004), Variations of 0.7–6.0 MeV electrons at geosynchronous orbit as a function of solar wind, *Space Weather*, *2*, S03006, doi:10.1029/2003SW000017.

Li, X., and M. Temerin (2001), The electron radiation belt, *Space Sci. Rev.*, *95*, 596.

Li, X., M. Temerin, D. N. Baker, G. D. Reeves, and D. Larson (2001), Quantitative prediction of radiation belt electrons at geostationary orbit based on solar wind measurements, *Geophys. Res. Lett.*, *28*, 1887.

O'Brien, T. P. (2001), Empirical analysis of storm-time energetic electron enhancements, Ph.D. thesis, Univ. of Calif., Los Angeles.

O'Brien, T. P., D. Sornette, and R. L. McPherron (2001), Statistical asynchronous regression: Determining the relationship between two quantities that are not measured simultaneously, *J. Geophys. Res.*, *106*, 13,247.

Onsager, T. G., R. Grubb, J. Kunches, L. Matheson, D. Speich, R. Zwickl, and H. Sauer (1996), Operational uses of the GOES energetic particle detectors, *Proc. SPIE Int. Soc. Opt. Eng.*, *2812*, 281.

Paulikas, G. A., and J. B. Blake (1979), Effects of the solar wind on magnetospheric dynamics: Energetic electrons at the synchronous orbit, in *Quantitative Modeling of Magnetospheric Processes*, *Geophys. Monogr. Ser.*, vol. *21*, edited by W. P. Olsen, p. 180, AGU, Washington, D. C.

Petrinec, S. M., and C. T. Russell (1993), External and internal influences on the size of the dayside terrestrial magnetopause, *Geophys. Res. Lett.*, *20*, 339.

Petrinec, S. M., and C. T. Russell (1996), Near-Earth magnetotail shape and size as determined from the magnetic flaring angle, *J. Geophys. Res.*, *101*, 137.

Spjeldvik, W. N., and P. L. Rothwell (1985), *Handbook of Geophysics and the Space Environment*, edited by A. S. Jursa, chap. 5, pp. 5.1–5.55, U.S. Air Force Syst. Command, Washington, D. C.

Stone, E. C., A. M. Frandsen, R. A. Mewaldt, E. R. Christian, D. Marglies, J. F. Ormes, and F. Snow (1998), The Advanced Composition Explorer, *Space Sci. Rev.*, *86*, 1.

Vampola, A. L. (1998), *Outer Zone Energetic Electron Environment Update*, IEEE Press, Piscataway, N. J.

Vette, J. I. (1966), Models of the trapped radiation environment, volume I: Inner zone protons and electrons, *NASA Tech. Pap. SP-3024*.

Vette, J. I. (1991), The AE-8 trapped electron model environment, *NASA Tech.*, 91-24.

Williams, D. J. (1966), A 27–day periodicity in outer zone trapped electron intensities, *J. Geophys. Res.*, *71*, 1815.

E. Burin des Roziers and X. Li, Department of Aerospace Engineering, University of Colorado, Boulder, CO 80303, USA. (ebdr@lasp.colorado.edu)